FERMILAB-PUB-13-432-E

Combination of measurements of the top-quark pair production cross section from the Tevatron Collider

T. Aaltonen[†],[21] V.M. Abazov[‡],[86] B. Abbott[‡],[117] B.S. Acharya[‡],[80] M. Adams[‡],[99] T. Adams[‡],[98] J.P. Agnew[‡],[95] G.D. Alexeev[‡],[86] G. Alkhazov[‡],[90] A. Alton[‡ii],[31] S. Amerio[†tt],[39] D. Amidei[†],[31] A. Anastassov[†v],[15] A. Annovi[†],[17] J. Antos[†],[12] G. Apollinari[†],[15] J.A. Appel[†],[15] T. Arisawa[†],[52] A. Artikov[†],[13] J. Asaadi[†],[47] W. Ashmanskas[†],[15] A. Askew[‡],[98] S. Atkins[‡],[107] B. Auerbach[†],[2] K. Augsten[‡],[62] A. Aurisano[†],[47] C. Avila[‡],[60] F. Azfar[†],[38] F. Badaud[‡],[65] W. Badgett[†],[15] T. Bae[†],[25] L. Bagby[‡],[15] B. Baldin[‡],[15] D.V. Bandurin[‡],[98] S. Banerjee[‡],[80] A. Barbaro-Galtieri[†],[26] E. Barberis[‡],[108] P. Baringer[‡],[106] V.E. Barnes[†],[43] B.A. Barnett[†],[23] P. Barria[†vv],[41] J.F. Bartlett[‡],[15] P. Bartos[†],[12] U. Bassler[‡],[70] M. Bauce[†tt],[39] V. Bazterra[‡],[99] A. Bean[‡],[106] F. Bedeschi[†],[41] M. Begalli[‡],[57] S. Behari[†],[15] L. Bellantoni[‡],[15] G. Bellettini[†uu],[41] J. Bellinger[†],[54] D. Benjamin[†],[14] A. Beretvas[†],[15] S.B. Beri[‡],[78] G. Bernardi[‡],[69] R. Bernhard[‡],[74] I. Bertram[‡],[93] M. Besançon[‡],[70] R. Beuselinck[‡],[94] P.C. Bhat[‡],[15] S. Bhatia[‡],[109] V. Bhatnagar[‡],[78] A. Bhatti[†],[45] K.R. Bland[†],[5] G. Blazey[‡],[100] S. Blessing[‡],[98] K. Bloom[‡],[110] B. Blumenfeld[†],[23] A. Bocci[†],[14] A. Bodek[†],[44] A. Boehnlein[‡],[15] D. Boline[‡],[114] E.E. Boos[‡],[88] G. Borissov[‡],[93] D. Bortoletto[†],[43] J. Boudreau[†],[42] A. Boveia[†],[11] A. Brandt[‡],[120] O. Brandt[‡],[75] L. Brigliadori[†ss],[6] R. Brock[‡],[32] C. Bromberg[†],[32] A. Bross[‡],[15] D. Brown[‡],[69] E. Brucken[†],[21] X.B. Bu[‡],[15] J. Budagov[†],[13] H.S. Budd[†],[44] M. Buehler[‡],[15] V. Buescher[‡],[76] V. Bunichev[‡],[88] S. Burdin[‡jj],[93] K. Burkett[†],[15] G. Busetto[†tt],[39] P. Bussey[†],[19] C.P. Buszello[‡],[92] P. Butti[†uu],[41] A. Buzatu[†],[19] A. Calamba[†],[10] E. Camacho-Pérez[‡],[83] S. Camarda[†],[4] M. Campanelli[†],[28] F. Canelli[†cc],[11] B. Carls[†],[22] D. Carlsmith[†],[54] R. Carosi[†],[41] S. Carrillo[†l],[16] B. Casal[†j],[9] M. Casarsa[†],[48] B.C.K. Casey[‡],[15] H. Castilla-Valdez[‡],[83] A. Castro[†ss],[6] P. Catastini[†],[20] S. Caughron[‡],[32] D. Cauz[†aaabbb],[48] V. Cavaliere[†],[22] M. Cavalli-Sforza[†],[4] A. Cerri[†e],[26] L. Cerrito[†q],[28] S. Chakrabarti[‡],[114] K.M. Chan[‡],[104] A. Chandra[‡],[122] E. Chapon[‡],[70] G. Chen[‡],[106] Y.C. Chen[†],[1] M. Chertok[†],[7] G. Chiarelli[†],[41] G. Chlachidze[†],[15] K. Cho[†],[25] S.W. Cho[‡],[82] S. Choi[‡],[82] D. Chokheli[†],[13] B. Choudhary[‡],[79] S. Cihangir[‡],[15] D. Claes[‡],[110] A. Clark[†],[18] C. Clarke[†],[53] J. Clutter[‡],[106] M.E. Convery[†],[15] J. Conway[†],[7] M. Cooke[‡],[15] W.E. Cooper[‡],[15] M. Corbo[†y],[15] M. Corcoran[‡],[122] M. Cordelli[†],[17] F. Couderc[‡],[70] M.-C. Cousinou[‡],[67] C.A. Cox[†],[7] D.J. Cox[†],[7] M. Cremonesi[†],[41] D. Cruz[†],[47] J. Cuevas[†x],[9] R. Culbertson[†],[15] D. Cutts[‡],[119] A. Das[‡],[96] N. d'Ascenzo[†u],[15] M. Datta[†fff],[15] G. Davies[‡],[94] P. de Barbaro[†],[44] S.J. de Jong[‡],[84,85] E. De La Cruz-Burelo[‡],[83] F. Déliot[‡],[70] R. Demina[‡],[44] L. Demortier[†],[45] M. Deninno[†],[6] D. Denisov[‡],[15] S.P. Denisov[‡],[89] M. D'Errico[†tt],[39] S. Desai[‡],[15] C. Deterre[‡kk],[75] K. DeVaughan[‡],[110] F. Devoto[†],[21] A. Di Canto[†uu],[41] B. Di Ruzza[†p],[15] H.T. Diehl[‡],[15] M. Diesburg[‡],[15] P.F. Ding[‡],[95] J.R. Dittmann[†],[5] A. Dominguez[‡],[110] S. Donati[†uu],[41] M. D'Onofrio[†],[27] M. Dorigo[†ccc],[48] A. Driutti[†aaabbb],[48] A. Dubey[‡],[79] L.V. Dudko[‡],[88] A. Duperrin[‡],[67] S. Dutt[‡],[78] M. Eads[‡],[100] K. Ebina[†],[52] R. Edgar[†],[31] D. Edmunds[‡],[32] A. Elagin[†],[47] J. Ellison[‡],[97] V.D. Elvira[‡],[15] Y. Enari[‡],[69] R. Erbacher[†],[7] S. Errede[†],[22] B. Esham[†],[22] H. Evans[‡],[102] V.N. Evdokimov[‡],[89] S. Farrington[†],[38] L. Feng[‡],[100] T. Ferbel[‡],[44] J.P. Fernández Ramos[†],[29] F. Fiedler[‡],[76] R. Field[†],[16] F. Filthaut[‡],[84,85] W. Fisher[‡],[32] H.E. Fisk[‡],[15] G. Flanagan[†s],[15] R. Forrest[†],[7] M. Fortner[‡],[100] H. Fox[‡],[93] M. Franklin[†],[20] J.C. Freeman[†],[15] H. Frisch[†],[11] S. Fuess[‡],[15] Y. Funakoshi[†],[52] C. Galloni[†uu],[41] P.H. Garbincius[‡],[15] A. Garcia-Bellido[‡],[44] J.A. García-González[‡],[83] A.F. Garfinkel[†],[43] P. Garosi[†vv],[41] V. Gavrilov[‡],[87] W. Geng[‡],[67,32] C.E. Gerber[‡],[99] H. Gerberich[†],[22] E. Gerchtein[†],[15] Y. Gershtein[‡],[111] S. Giagu[†],[46] V. Giakoumopoulou[†],[3] K. Gibson[†],[42] C.M. Ginsburg[†],[15] G. Ginther[‡],[15,44] N. Giokaris[†],[3] P. Giromini[†],[17] G. Giurgiu[†],[23] V. Glagolev[†],[13] D. Glenzinski[†],[15] M. Gold[†],[34] D. Goldin[†],[47] A. Golossanov[†],[15] G. Golovanov[‡],[86] G. Gomez[†],[9] G. Gomez-Ceballos[†],[30] M. Goncharov[†],[30] O. González López[†],[29] I. Gorelov[†],[34] A.T. Goshaw[†],[14] K. Goulianos[†],[45] E. Gramellini[†],[6] P.D. Grannis[‡],[114] S. Greder[‡],[71] H. Greenlee[‡],[15] G. Grenier[‡],[72] S. Grinstein[†],[4] Ph. Gris[‡],[65] J.-F. Grivaz[‡],[68] A. Grohsjean[‡kk],[70] C. Grosso-Pilcher[†],[11] R.C. Group[†],[51,15] S. Grünendahl[‡],[15] M.W. Grünewald[‡],[81] T. Guillemin[‡],[68] J. Guimaraes da Costa[†],[20] G. Gutierrez[‡],[15] P. Gutierrez[‡],[117] S.R. Hahn[†],[15] J. Haley[‡],[117] J.Y. Han[†],[44] L. Han[‡],[59] F. Happacher[†],[17] K. Hara[†],[49] K. Harder[‡],[95] M. Hare[†],[50] A. Harel[‡],[44] R.F. Harr[†],[53] T. Harrington-Taber[†m],[15] K. Hatakeyama[†],[5] J.M. Hauptman[‡],[105] C. Hays[†],[38] J. Hays[‡],[94] T. Head[‡],[95] T. Hebbeker[‡],[73] D. Hedin[‡],[100] H. Hegab[‡],[118] J. Heinrich[†],[40] A.P. Heinson[‡],[97] U. Heintz[‡],[119] C. Hensel[‡],[75] I. Heredia-De La Cruz[‡ll],[83] M. Herndon[†],[54] K. Herner[‡],[15] G. Hesketh[‡nn],[95] M.D. Hildreth[‡],[104] R. Hirosky[‡],[123] T. Hoang[‡],[98] J.D. Hobbs[‡],[114] A. Hocker[†],[15] B. Hoeneisen[‡],[64] J. Hogan[‡],[122] M. Hohlfeld[‡],[76] J.L. Holzbauer[‡],[109] Z. Hong[†],[47] W. Hopkins[†f],[15] S. Hou[†],[1] I. Howley[‡],[120] Z. Hubacek[‡],[62,70] R.E. Hughes[†],[35] U. Husemann[†],[55] M. Hussein[†aa],[32] J. Huston[†],[32] V. Hynek[‡],[62] I. Iashvili[‡],[113] Y. Ilchenko[‡],[121] R. Illingworth[‡],[15] G. Introzzi[†xxyy],[41] M. Iori[†zz],[46] A.S. Ito[‡],[15] A. Ivanov[†o],[7] S. Jabeen[‡],[119] M. Jaffré[‡],[68] E. James[†],[15] D. Jang[†],[10] A. Jayasinghe[‡],[117] B. Jayatilaka[†],[15] E.J. Jeon[†],[25] M.S. Jeong[‡],[82] R. Jesik[‡],[94] P. Jiang[‡],[59] S. Jindariani[†],[15] K. Johns[‡],[96] E. Johnson[‡],[32] M. Johnson[‡],[15] A. Jonckheere[‡],[15] M. Jones[†],[43]

Operated by Fermi Research Alliance, LLC under Contract No. De-AC02-07CH11359 with the United States Department of Energy.

P. Jonsson[‡,94] K.K. Joo[†,25] J. Joshi[‡,97] S.Y. Jun[†,10] A.W. Jung[‡,15] T.R. Junk[†,15] A. Juste[‡,91] E. Kajfasz[‡,67] M. Kambeitz[†,24] T. Kamon[†,25,47] P.E. Karchin[†,53] D. Karmanov[‡,88] A. Kasmi[†,5] Y. Kato[†n,37] I. Katsanos[‡,110] R. Kehoe[‡,121] S. Kermiche[‡,67] W. Ketchum[†gg,11] J. Keung[†,40] N. Khalatyan[‡,15] A. Khanov[‡,118] A. Kharchilava[‡,113] Y.N. Kharzheev[‡,86] B. Kilminster[†cc,15] D.H. Kim[†,25] H.S. Kim[†,25] J.E. Kim[†,25] M.J. Kim[†,17] S.H. Kim[†,49] S.B. Kim[†,25] Y.J. Kim[†,25] Y.K. Kim[†,11] N. Kimura[†,52] M. Kirby[†,15] I. Kiselevich[‡,87] K. Knoepfel[†,15] J.M. Kohli[‡,78] K. Kondo[†,52,*] D.J. Kong[†,25] J. Konigsberg[†,16] A.V. Kotwal[†,14] A.V. Kozelov[‡,89] J. Kraus[‡,109] M. Kreps[†,24] J. Kroll[†,40] M. Kruse[†,14] T. Kuhr[†,24] A. Kumar[‡,113] A. Kupco[‡,63] M. Kurata[†,49] T. Kurča[‡,72] V.A. Kuzmin[‡,88] A.T. Laasanen[†,43] S. Lammel[†,15] S. Lammers[‡,102] M. Lancaster[†,28] K. Lannon[†w,35] G. Latino[†vv,41] P. Lebrun[‡,72] H.S. Lee[‡,82] H.S. Lee[†,25] J.S. Lee[†,25] S.W. Lee[‡,105] W.M. Lee[‡,15] X. Lei[‡,96] J. Lellouch[‡,69] S. Leo[†,41] S. Leone[†,41] J.D. Lewis[†,15] D. Li[‡,69] H. Li[‡,123] L. Li[‡,97] Q.Z. Li[‡,15] J.K. Lim[‡,82] A. Limosani[†r,14] D. Lincoln[‡,15] J. Linnemann[‡,32] V.V. Lipaev[‡,89] E. Lipeles[†,40] R. Lipton[‡,15] A. Lister[†a,18] H. Liu[†,51] H. Liu[‡,121] Q. Liu[†,43] T. Liu[†,15] Y. Liu[‡,59] A. Lobodenko[‡,90] S. Lockwitz[†,55] A. Loginov[†,55] M. Lokajicek[‡,63] R. Lopes de Sa[‡,114] D. Lucchesi[†tt,39] A. Lucà[†,17] J. Lueck[†,24] P. Lujan[†,26] P. Lukens[†,15] R. Luna-Garcia[‡oo,83] G. Lungu[†,45] A.L. Lyon[‡,15] J. Lys[†,26] R. Lysak[†d,12] A.K.A. Maciel[‡,56] R. Madar[‡,74] R. Madrak[†,15] P. Maestro[†vv,41] R. Magaña-Villalba[‡,83] S. Malik[†,45] S. Malik[‡,110] V.L. Malyshev[‡,86] G. Manca[†b,27] A. Manousakis-Katsikakis[†,3] J. Mansour[‡,75] L. Marchese[†hh,6] F. Margaroli[†,46] P. Marino[†ww,41] J. Martínez-Ortega[‡,83] M. Martínez[†,4] K. Matera[†,22] M.E. Mattson[†,53] A. Mazzacane[†,15] P. Mazzanti[†,6] R. McCarthy[‡,114] C.L. McGivern[‡,95] R. McNulty[†i,27] A. Mehta[†,27] P. Mehtala[†,21] M.M. Meijer[‡,84,85] A. Melnitchouk[‡,15] D. Menezes[‡,100] P.G. Mercadante[‡,58] M. Merkin[‡,88] C. Mesropian[†,45] A. Meyer[‡,73] J. Meyer[‡qq,75] T. Miao[†,15] F. Miconi[‡,71] D. Mietlicki[†,31] A. Mitra[†,1] H. Miyake[†,49] S. Moed[†,15] N. Moggi[†,6] N.K. Mondal[‡,80] C.S. Moon[†y,15] R. Moore[†ddee,15] M.J. Morello[†ww,41] A. Mukherjee[†,15] M. Mulhearn[‡,123] Th. Muller[†,24] P. Murat[†,15] M. Mussini[†ss,6] J. Nachtman[†m,15] Y. Nagai[†,49] J. Naganoma[†,52] E. Nagy[‡,67] I. Nakano[†,36] A. Napier[†,50] M. Narain[‡,119] R. Nayyar[‡,96] H.A. Neal[‡,31] J.P. Negret[‡,60] J. Nett[†,47] C. Neu[†,51] P. Neustroev[‡,90] H.T. Nguyen[‡,123] T. Nigmanov[†,42] L. Nodulman[†,2] S.Y. Noh[†,25] O. Norniella[†,22] T. Nunnemann[‡,77] L. Oakes[†,38] S.H. Oh[†,14] Y.D. Oh[†,25] I. Oksuzian[†,51] T. Okusawa[†,37] R. Orava[†,21] J. Orduna[‡,122] L. Ortolan[†,4] N. Osman[‡,67] J. Osta[‡,104] C. Pagliarone[†,48] A. Pal[‡,120] E. Palencia[†e,9] P. Palni[†,34] V. Papadimitriou[†,15] N. Parashar[‡,103] V. Parihar[‡,119] S.K. Park[‡,82] W. Parker[†,54] R. Partridge[‡mm,119] N. Parua[‡,102] A. Patwa[‡rr,115] G. Pauletta[†aaabbb,48] M. Paulini[†,10] C. Paus[†,30] B. Penning[‡,15] M. Perfilov[‡,88] Y. Peters[‡,75] K. Petridis[‡,95] G. Petrillo[‡,44] P. Pétroff[‡,68] T.J. Phillips[†,14] G. Piacentino[†,41] E. Pianori[†,40] J. Pilot[†,7] K. Pitts[†,22] C. Plager[†,8] M.-A. Pleier[‡,115] V.M. Podstavkov[‡,15] L. Pondrom[†,54] A.V. Popov[‡,89] S. Poprocki[†f,15] K. Potamianos[†,26] A. Pranko[†,26] M. Prewitt[‡,122] D. Price[‡,95] N. Prokopenko[‡,89] F. Prokoshin[†z,13] F. Ptohos[†g,17] G. Punzi[†uu,41] J. Qian[‡,31] A. Quadt[‡,75] B. Quinn[‡,109] N. Ranjan[†,43] P.N. Ratoff[‡,93] I. Razumov[‡,89] I. Redondo Fernández[†,29] P. Renton[†,38] M. Rescigno[†,46] F. Rimondi[†,6,*] I. Ripp-Baudot[‡,71] L. Ristori[†,41,15] F. Rizatdinova[‡,118] A. Robson[†,19] T. Rodriguez[†,40] S. Rolli[†h,50] M. Rominsky[‡,15] M. Ronzani[†uu,41] R. Roser[†,15] J.L. Rosner[†,11] A. Ross[‡,93] C. Royon[‡,70] P. Rubinov[‡,15] R. Ruchti[‡,104] F. Ruffini[†vv,41] A. Ruiz[†,9] J. Russ[†,10] V. Rusu[†,15] G. Sajot[‡,66] W.K. Sakumoto[†,44] Y. Sakurai[†,52] A. Sánchez-Hernández[‡,83] M.P. Sanders[‡,77] L. Santi[†aaabbb,48] A.S. Santos[‡pp,56] K. Sato[†,49] G. Savage[‡,15] V. Saveliev[†u,15] A. Savoy-Navarro[†y,15] L. Sawyer[‡,107] T. Scanlon[‡,94] R.D. Schamberger[‡,114] Y. Scheglov[‡,90] H. Schellman[‡,101] P. Schlabach[†,15] E.E. Schmidt[†,15] C. Schwanenberger[‡,95] T. Schwarz[†,31] R. Schwienhorst[‡,32] L. Scodellaro[†,9] F. Scuri[†,41] S. Seidel[†,34] Y. Seiya[†,37] J. Sekaric[‡,106] A. Semenov[†,13] H. Severini[‡,117] F. Sforza[†uu,41] E. Shabalina[‡,75] S.Z. Shalhout[†,7] V. Shary[‡,70] S. Shaw[‡,32] A.A. Shchukin[‡,89] T. Shears[†,27] P.F. Shepard[†,42] M. Shimojima[†t,49] M. Shochet[†,11] I. Shreyber-Tecker[†,33] V. Simak[‡,62] A. Simonenko[†,13] P. Skubic[‡,117] P. Slattery[‡,44] K. Sliwa[†,50] D. Smirnov[‡,104] J.R. Smith[†,7] F.D. Snider[†,15] G.R. Snow[‡,110] J. Snow[‡,116] S. Snyder[‡,115] S. Söldner-Rembold[‡,95] H. Song[†,42] L. Sonnenschein[‡,73] V. Sorin[†,4] K. Soustruznik[‡,61] R. St. Denis[†,19] M. Stancari[†,15] J. Stark[‡,66] D. Stentz[†v,15] D.A. Stoyanova[‡,89] M. Strauss[‡,117] J. Strologas[†,34] Y. Sudo[†,49] A. Sukhanov[†,15] I. Suslov[†,13] L. Suter[‡,95] P. Svoisky[‡,117] K. Takemasa[†,49] Y. Takeuchi[†,49] J. Tang[†,11] M. Tecchio[†,31] P.K. Teng[†,1] J. Thom[†f,15] E. Thomson[†,40] V. Thukral[†,47] M. Titov[‡,70] D. Toback[†,47] S. Tokar[†,12] V.V. Tokmenin[‡,86] K. Tollefson[†,32] T. Tomura[†,49] D. Tonelli[†e,15] S. Torre[†,17] D. Torretta[†,15] P. Totaro[†,39] M. Trovato[†ww,41] Y.-T. Tsai[‡,44] D. Tsybychev[‡,114] B. Tuchming[‡,70] C. Tully[‡,112] F. Ukegawa[†,49] S. Uozumi[†,25] L. Uvarov[‡,90] S. Uvarov[‡,90] S. Uzunyan[‡,100] R. Van Kooten[‡,102] W.M. van Leeuwen[‡,84] N. Varelas[‡,99] E.W. Varnes[‡,96] I.A. Vasilyev[‡,89] F. Vázquez[†l,16] G. Velev[†,15] C. Vellidis[†,15] A.Y. Verkheev[‡,86] C. Vernieri[†ww,41] L.S. Vertogradov[‡,86] M. Verzocchi[‡,15] M. Vesterinen[‡,95] M. Vidal[†,43] D. Vilanova[‡,70] R. Vilar[†,9] J. Vizán[†bb,9] M. Vogel[†,34] P. Vokac[‡,62] G. Volpi[†,17] P. Wagner[†,40] H.D. Wahl[‡,98] R. Wallny[†j,15] M.H.L.S. Wang[‡,15] S.M. Wang[†,1] J. Warchol[‡,104] D. Waters[†,28]

Operated by Fermi Research Alliance, LLC under Contract No. De-AC02-07CH11359 with the United States Department of Energy.

G. Watts[‡],[124] M. Wayne[‡],[104] J. Weichert[‡],[76] L. Welty-Rieger[‡],[101] W.C. Wester III[†],[15] D. Whiteson[†c],[40] A.B. Wicklund[†],[2] S. Wilbur[†],[7] H.H. Williams[†],[40] M.R.J. Williams[‡],[102] G.W. Wilson[‡],[106] J.S. Wilson[†],[31] P. Wilson[†],[15] B.L. Winer[†],[35] P. Wittich[†f],[15] M. Wobisch[‡],[107] S. Wolbers[†],[15] H. Wolfe[†],[35] D.R. Wood[‡],[108] T. Wright[†],[31] X. Wu[†],[18] Z. Wu[†],[5] T.R. Wyatt[‡],[95] Y. Xie[‡],[15] R. Yamada[‡],[15] K. Yamamoto[†],[37] D. Yamato[†],[37] S. Yang[‡],[59] T. Yang[†],[15] U.K. Yang[†],[25] Y.C. Yang[†],[25] W.-M. Yao[†],[26] T. Yasuda[‡],[15] Y.A. Yatsunenko[‡],[86] W. Ye[‡],[114] Z. Ye[‡],[15] G.P. Yeh[†],[15] K. Yi[†m],[15] H. Yin[‡],[15] K. Yip[‡],[115] J. Yoh[†],[15] K. Yorita[†],[52] T. Yoshida[†k],[37] S.W. Youn[‡],[15] G.B. Yu[†],[14] I. Yu[†],[25] J.M. Yu[‡],[31] A.M. Zanetti[†],[48] Y. Zeng[†],[14] J. Zennamo[‡],[113] T.G. Zhao[‡],[95] B. Zhou[‡],[31] C. Zhou[†],[14] J. Zhu[‡],[31] M. Zielinski[‡],[44] D. Zieminska[‡],[102] L. Zivkovic[‡],[69] and S. Zucchelli[†ss6]

(CDF Collaboration),[†]

(D0 Collaboration),[‡]

[1]*Institute of Physics, Academia Sinica, Taipei, Taiwan 11529, Republic of China*
[2]*Argonne National Laboratory, Argonne, Illinois 60439, USA*
[3]*University of Athens, 157 71 Athens, Greece*
[4]*Institut de Fisica d'Altes Energies, ICREA, Universitat Autonoma de Barcelona, E-08193, Bellaterra (Barcelona), Spain*
[5]*Baylor University, Waco, Texas 76798, USA*
[6]*Istituto Nazionale di Fisica Nucleare Bologna, [ss] University of Bologna, I-40127 Bologna, Italy*
[7]*University of California, Davis, Davis, California 95616, USA*
[8]*University of California, Los Angeles, Los Angeles, California 90024, USA*
[9]*Instituto de Fisica de Cantabria, CSIC-University of Cantabria, 39005 Santander, Spain*
[10]*Carnegie Mellon University, Pittsburgh, Pennsylvania 15213, USA*
[11]*Enrico Fermi Institute, University of Chicago, Chicago, Illinois 60637, USA*
[12]*Comenius University, 842 48 Bratislava, Slovakia; Institute of Experimental Physics, 040 01 Kosice, Slovakia*
[13]*Joint Institute for Nuclear Research, RU-141980 Dubna, Russia*
[14]*Duke University, Durham, North Carolina 27708, USA*
[15]*Fermi National Accelerator Laboratory, Batavia, Illinois 60510, USA*
[16]*University of Florida, Gainesville, Florida 32611, USA*
[17]*Laboratori Nazionali di Frascati, Istituto Nazionale di Fisica Nucleare, I-00044 Frascati, Italy*
[18]*University of Geneva, CH-1211 Geneva 4, Switzerland*
[19]*Glasgow University, Glasgow G12 8QQ, United Kingdom*
[20]*Harvard University, Cambridge, Massachusetts 02138, USA*
[21]*Division of High Energy Physics, Department of Physics, University of Helsinki, FIN-00014, Helsinki, Finland; Helsinki Institute of Physics, FIN-00014, Helsinki, Finland*
[22]*University of Illinois, Urbana, Illinois 61801, USA*
[23]*The Johns Hopkins University, Baltimore, Maryland 21218, USA*
[24]*Institut für Experimentelle Kernphysik, Karlsruhe Institute of Technology, D-76131 Karlsruhe, Germany*
[25]*Center for High Energy Physics: Kyungpook National University, Daegu 702-701, Korea; Seoul National University, Seoul 151-742, Korea; Sungkyunkwan University, Suwon 440-746, Korea; Korea Institute of Science and Technology Information, Daejeon 305-806, Korea; Chonnam National University, Gwangju 500-757, Korea; Chonbuk National University, Jeonju 561-756, Korea; Ewha Womans University, Seoul, 120-750, Korea*
[26]*Ernest Orlando Lawrence Berkeley National Laboratory, Berkeley, California 94720, USA*
[27]*University of Liverpool, Liverpool L69 7ZE, United Kingdom*
[28]*University College London, London WC1E 6BT, United Kingdom*
[29]*Centro de Investigaciones Energeticas Medioambientales y Tecnologicas, E-28040 Madrid, Spain*
[30]*Massachusetts Institute of Technology, Cambridge, Massachusetts 02139, USA*
[31]*University of Michigan, Ann Arbor, Michigan 48109, USA*
[32]*Michigan State University, East Lansing, Michigan 48824, USA*
[33]*Institution for Theoretical and Experimental Physics, ITEP, Moscow 117259, Russia*
[34]*University of New Mexico, Albuquerque, New Mexico 87131, USA*
[35]*The Ohio State University, Columbus, Ohio 43210, USA*
[36]*Okayama University, Okayama 700-8530, Japan*
[37]*Osaka City University, Osaka 558-8585, Japan*
[38]*University of Oxford, Oxford OX1 3RH, United Kingdom*
[39]*Istituto Nazionale di Fisica Nucleare, Sezione di Padova, [tt] University of Padova, I-35131 Padova, Italy*
[40]*University of Pennsylvania, Philadelphia, Pennsylvania 19104, USA*
[41]*Istituto Nazionale di Fisica Nucleare Pisa, [uu] University of Pisa, [vv] University of Siena, [ww] Scuola Normale Superiore, I-56127 Pisa, Italy, [xx] INFN Pavia, I-27100 Pavia, Italy, [yy] University of Pavia, I-27100 Pavia, Italy*

Operated by Fermi Research Alliance, LLC under Contract No. De-AC02-07CH11359 with the United States Department of Energy.

[42] University of Pittsburgh, Pittsburgh, Pennsylvania 15260, USA
[43] Purdue University, West Lafayette, Indiana 47907, USA
[44] University of Rochester, Rochester, New York 14627, USA
[45] The Rockefeller University, New York, New York 10065, USA
[46] Istituto Nazionale di Fisica Nucleare, Sezione di Roma 1,
[zz] Sapienza Università di Roma, I-00185 Roma, Italy
[47] Mitchell Institute for Fundamental Physics and Astronomy,
Texas A&M University, College Station, Texas 77843, USA
[48] Istituto Nazionale di Fisica Nucleare Trieste, [aaa] Gruppo Collegato di Udine,
[bbb] University of Udine, I-33100 Udine, Italy, [ccc] University of Trieste, I-34127 Trieste, Italy
[49] University of Tsukuba, Tsukuba, Ibaraki 305, Japan
[50] Tufts University, Medford, Massachusetts 02155, USA
[51] University of Virginia, Charlottesville, Virginia 22906, USA
[52] Waseda University, Tokyo 169, Japan
[53] Wayne State University, Detroit, Michigan 48201, USA
[54] University of Wisconsin, Madison, Wisconsin 53706, USA
[55] Yale University, New Haven, Connecticut 06520, USA
[56] LAFEX, Centro Brasileiro de Pesquisas Físicas, Rio de Janeiro, Brazil
[57] Universidade do Estado do Rio de Janeiro, Rio de Janeiro, Brazil
[58] Universidade Federal do ABC, Santo André, Brazil
[59] University of Science and Technology of China, Hefei, People's Republic of China
[60] Universidad de los Andes, Bogotá, Colombia
[61] Charles University, Faculty of Mathematics and Physics,
Center for Particle Physics, Prague, Czech Republic
[62] Czech Technical University in Prague, Prague, Czech Republic
[63] Institute of Physics, Academy of Sciences of the Czech Republic, Prague, Czech Republic
[64] Universidad San Francisco de Quito, Quito, Ecuador
[65] LPC, Université Blaise Pascal, CNRS/IN2P3, Clermont, France
[66] LPSC, Université Joseph Fourier Grenoble 1, CNRS/IN2P3,
Institut National Polytechnique de Grenoble, Grenoble, France
[67] CPPM, Aix-Marseille Université, CNRS/IN2P3, Marseille, France
[68] LAL, Université Paris-Sud, CNRS/IN2P3, Orsay, France
[69] LPNHE, Universités Paris VI and VII, CNRS/IN2P3, Paris, France
[70] CEA, Irfu, SPP, Saclay, France
[71] IPHC, Université de Strasbourg, CNRS/IN2P3, Strasbourg, France
[72] IPNL, Université Lyon 1, CNRS/IN2P3, Villeurbanne, France and Université de Lyon, Lyon, France
[73] III. Physikalisches Institut A, RWTH Aachen University, Aachen, Germany
[74] Physikalisches Institut, Universität Freiburg, Freiburg, Germany
[75] II. Physikalisches Institut, Georg-August-Universität Göttingen, Göttingen, Germany
[76] Institut für Physik, Universität Mainz, Mainz, Germany
[77] Ludwig-Maximilians-Universität München, München, Germany
[78] Panjab University, Chandigarh, India
[79] Delhi University, Delhi, India
[80] Tata Institute of Fundamental Research, Mumbai, India
[81] University College Dublin, Dublin, Ireland
[82] Korea Detector Laboratory, Korea University, Seoul, Korea
[83] CINVESTAV, Mexico City, Mexico
[84] Nikhef, Science Park, Amsterdam, the Netherlands
[85] Radboud University Nijmegen, Nijmegen, the Netherlands
[86] Joint Institute for Nuclear Research, Dubna, Russia
[87] Institute for Theoretical and Experimental Physics, Moscow, Russia
[88] Moscow State University, Moscow, Russia
[89] Institute for High Energy Physics, Protvino, Russia
[90] Petersburg Nuclear Physics Institute, St. Petersburg, Russia
[91] Institució Catalana de Recerca i Estudis Avançats (ICREA) and Institut de Física d'Altes Energies (IFAE), Barcelona, Spain
[92] Uppsala University, Uppsala, Sweden
[93] Lancaster University, Lancaster LA1 4YB, United Kingdom
[94] Imperial College London, London SW7 2AZ, United Kingdom
[95] The University of Manchester, Manchester M13 9PL, United Kingdom
[96] University of Arizona, Tucson, Arizona 85721, USA
[97] University of California Riverside, Riverside, California 92521, USA
[98] Florida State University, Tallahassee, Florida 32306, USA
[99] University of Illinois at Chicago, Chicago, Illinois 60607, USA
[100] Northern Illinois University, DeKalb, Illinois 60115, USA

Operated by Fermi Research Alliance, LLC under Contract No. De-AC02-07CH11359 with the United States Department of Energy.

[101]Northwestern University, Evanston, Illinois 60208, USA
[102]Indiana University, Bloomington, Indiana 47405, USA
[103]Purdue University Calumet, Hammond, Indiana 46323, USA
[104]University of Notre Dame, Notre Dame, Indiana 46556, USA
[105]Iowa State University, Ames, Iowa 50011, USA
[106]University of Kansas, Lawrence, Kansas 66045, USA
[107]Louisiana Tech University, Ruston, Louisiana 71272, USA
[108]Northeastern University, Boston, Massachusetts 02115, USA
[109]University of Mississippi, University, Mississippi 38677, USA
[110]University of Nebraska, Lincoln, Nebraska 68588, USA
[111]Rutgers University, Piscataway, New Jersey 08855, USA
[112]Princeton University, Princeton, New Jersey 08544, USA
[113]State University of New York, Buffalo, New York 14260, USA
[114]State University of New York, Stony Brook, New York 11794, USA
[115]Brookhaven National Laboratory, Upton, New York 11973, USA
[116]Langston University, Langston, Oklahoma 73050, USA
[117]University of Oklahoma, Norman, Oklahoma 73019, USA
[118]Oklahoma State University, Stillwater, Oklahoma 74078, USA
[119]Brown University, Providence, Rhode Island 02912, USA
[120]University of Texas, Arlington, Texas 76019, USA
[121]Southern Methodist University, Dallas, Texas 75275, USA
[122]Rice University, Houston, Texas 77005, USA
[123]University of Virginia, Charlottesville, Virginia 22904, USA
[124]University of Washington, Seattle, Washington 98195, USA

(Dated: September 27th, 2013)

We combine six measurements of the inclusive top-quark pair ($t\bar{t}$) production cross section ($\sigma_{t\bar{t}}$) from data collected with the CDF and D0 detectors at the Fermilab Tevatron with proton anti-proton collisions at $\sqrt{s} = 1.96$ TeV. The data correspond to integrated luminosities of up to 8.8 fb^{-1}. We obtain a value of $\sigma_{t\bar{t}} = 7.60 \pm 0.41$ pb for a top-quark mass of $m_t = 172.5$ GeV. The contributions to the uncertainty are 0.20 pb from statistical sources, 0.29 pb from systematic sources, and 0.21 pb from the uncertainty on the integrated luminosity. The result is in good agreement with the standard model expectation of $7.35^{+0.28}_{-0.33}$ pb at NNLO+NNLL in pertubative QCD.

PACS numbers: 14.65.Ha, 12.38.Qk, 13.85.Qk

I. INTRODUCTION

The top quark, the most massive elementary particle to date and the final member of the three families of quarks of the standard model (SM), was first observed in 1995 by the CDF and D0 experiments at the Fermilab Tevatron proton-antiproton ($p\bar{p}$) collider [1, 2]. The large mass of the top quark of $m_t = 173.20 \pm 0.87$ GeV [3] and its short

*Deceased
†With visitors from [a]University of British Columbia, Vancouver, BC V6T 1Z1, Canada, [b]Istituto Nazionale di Fisica Nucleare, Sezione di Cagliari, 09042 Monserrato (Cagliari), Italy, [c]University of California Irvine, Irvine, CA 92697, USA, [d]Institute of Physics, Academy of Sciences of the Czech Republic, 182 21, Czech Republic, [e]CERN, CH-1211 Geneva, Switzerland, [f]Cornell University, Ithaca, NY 14853, USA, [g]University of Cyprus, Nicosia CY-1678, Cyprus, [h]Office of Science, U.S. Department of Energy, Washington, DC 20585, USA, [i]University College Dublin, Dublin 4, Ireland, [j]ETH, 8092 Zürich, Switzerland, [k]University of Fukui, Fukui City, Fukui Prefecture, Japan 910-0017, [l]Universidad Iberoamericana, Lomas de Santa Fe, México, C.P. 01219, Distrito Federal, [m]University of Iowa, Iowa City, IA 52242, USA, [n]Kinki University, Higashi-Osaka City, Japan 577-8502, [o]Kansas State University, Manhattan, KS 66506, USA, [p]Brookhaven National Laboratory, Upton, NY 11973, USA, [q]Queen Mary, University of London, London, E1 4NS, United Kingdom, [r]University of Melbourne, Victoria 3010, Australia, [s]Muons, Inc., Batavia, IL 60510, USA, [t]Nagasaki Institute of Applied Science, Nagasaki 851-0193, Japan, [u]National Research Nuclear University, Moscow 115409, Russia, [v]Northwestern University, Evanston, IL 60208, USA, [w]University of Notre Dame, Notre Dame, IN 46556, USA, [x]Universidad de Oviedo, E-33007 Oviedo, Spain, [y]CNRS-IN2P3, Paris, F-75205 France, [z]Universidad Tecnica Federico Santa Maria, 110v Valparaiso, Chile, [aa]The University of Jordan, Amman 11942, Jordan, [bb]Universite catholique de Louvain, 1348 Louvain-La-Neuve, Belgium, [cc]University of Zürich, 8006 Zürich, Switzerland, [dd]Massachusetts General Hospital, Boston, MA 02114 USA, [ee]Harvard Medical School, Boston, MA 02114 USA, [ff]Hampton University, Hampton, VA 23668, USA, [gg]Los Alamos National Laboratory, Los Alamos, NM 87544, USA, [hh]Università degli Studi di Napoli Federico I, I-80138 Napoli, Italy
‡With visitors from [ii]Augustana College, Sioux Falls, SD, USA, [jj]The University of Liverpool, Liverpool, UK, [kk]DESY, Hamburg, Germany, [ll]Universidad Michoacana de San Nicolas de Hidalgo, Morelia, Mexico, [mm]SLAC, Menlo Park, CA, USA, [nn]University College London, London, UK, [oo]Centro de Investigacion en Computacion - IPN, Mexico City, Mexico, [pp]Universidade Estadual Paulista, São Paulo, Brazil, [qq]Karlsruher Institut für Technologie (KIT) - Steinbuch Centre for Computing (SCC), [rr]Office of Science, U.S. Department of Energy, Washington, D.C. 20585, USA

Operated by Fermi Research Alliance, LLC under Contract No. De-AC02-07CH11359 with the United States Department of Energy.

lifetime of approximately 10^{-25} s [4, 5] are of special interest. The lifetime is far shorter than the hadronization time, and provides the opportunity to study the properties of essentially a bare quark. The large mass suggests that the top quark may play a special role in the mechanism of electroweak symmetry breaking, and thereby provide sensitivity to probe a broad class of SM extensions. In addition, with the recent discovery of a Higgs boson [6, 7], the properties of the top quark are expected to be related to the stability of the vacuum in the universe [8].

The properties of the top quark can be assessed through precise determinations of its production mechanisms and decay rates, in comparison to SM expectations. Particles and couplings predicted by extensions of the SM can affect the observed production cross sections of top quarks. For example, the observed top-quark pair ($t\bar{t}$) production cross section in all of the experimental final states may be enhanced above the SM expectation by the production of new resonances [9, 10], or the observed production cross section in some of the experimental final states may be altered from the SM expectation by top quark decay into new channels, such as a hypothesized charged Higgs boson and b quark [11, 12].

In this article, we report on the first combination of measurements by the CDF and D0 experiments at the Fermilab Tevatron of the inclusive $t\bar{t}$ production cross section ($\sigma_{t\bar{t}}$), with the goal of reducing the experimental uncertainty and thereby providing a better test of the SM prediction. The inclusive $t\bar{t}$ cross section has also been measured at the LHC at different center of mass energies [13, 14]. In the remainder of this section, the status of the theoretical predictions and the experimental signatures of the $t\bar{t}$ final states are described. Section II reviews all six measurements, reports the first combination of the four CDF results, and reviews the combination of the two D0 results [15]. The categories of systematic uncertainties and their correlations among the measurements are detailed in Sec. III. The first combination of the CDF and D0 measurements is reported in Sec. IV and conclusions are drawn in Sec. V.

A. Predictions for the $t\bar{t}$ production cross section

According to the SM, production of top quarks at hadron colliders takes place through strong interactions that produce $t\bar{t}$, or through electroweak processes that produce a single top quark. At the Tevatron $p\bar{p}$ collider, with a center of mass energy of $\sqrt{s} = 1.96$ TeV, top quark production occurs mainly through $t\bar{t}$ production, which is the focus of this article. The contribution to $t\bar{t}$ production is approximately 85% from quark-antiquark annihilation ($q\bar{q} \to t\bar{t}$) and 15% from gluon-gluon fusion ($gg \to t\bar{t}$).

SM predictions for inclusive $t\bar{t}$ production at the Tevatron, calculated to different orders in perturbative quantum chromodynamics (QCD), are available in Refs. [16–24]. The first calculations at full next-to-leading-order (NLO) QCD were performed before the discovery of the top quark [16], and have been updated using the more recent CTEQ6.6 parton distribution functions (PDF) [17]. These full NLO calculations were further improved by adding resummations of logarithmic corrections to the cross section from higher-order soft-gluon radiation, in particular by including next-to-leading logarithmic (NLL) soft-gluon resummation [18] and the more recent PDF [19]. Also available are NLO calculations with soft-gluon resummation to next-to-next-to-leading logarithmic (NNLL) accuracy, and approximations at next-to-next-to-leading-order (NNLO) obtained by re-expanding the result from NLO+NNLL in a fixed-order series in the strong coupling constant α_s ($\mathrm{NNLO_{approx}}$) [20–23]. Differences between these calculations include using a momentum-space or N-space approach, and resummation of the total cross section or integration of the differential cross section over phase space.

The computation at full NNLO QCD was performed for the first time in 2013 [24], with an uncertainty on $\sigma_{t\bar{t}}$ of approximately 4% when matched with NNLL soft-gluon resummation. To estimate the uncertainty on $\sigma_{t\bar{t}}$ for a given top-quark mass, the factorization and renormalization scales are changed by factors of two or one half relative to their nominal values. The sensitivity to choice of PDF is evaluated by changing all the PDF parameters within their uncertainties [17]. The predicted values of $\sigma_{t\bar{t}}$ and their corresponding uncertainties, calculated with the Top++ program [25], are provided in Table I at NLO, NLO+NLL, and NNLO+NNLL. The top-quark mass for these calculations is set to $m_t = 172.5$ GeV, with the PDF set corresponding to either MSTW2008nlo68cl or MSTW2008nnlo68cl [26].

We use the full NNLO+NNLL prediction as the default value for comparison with the measurements since it has the smallest uncertainty. The benefit of the recent theoretical advance to full NNLO+NNLL consists of an approximate 4% increase of the cross section and a reduction in the scale uncertainty with respect to the NLO+NLL prediction.

TABLE I: SM predictions of $\sigma_{t\bar{t}}$ at different orders in perturbative QCD, using Top++ [25].

Calculation	$\sigma_{t\bar{t}}$ (pb)	$\Delta\sigma_{\mathrm{scale}}$ (pb)	$\Delta\sigma_{\mathrm{PDF}}$ (pb)
NLO	6.85	$^{+0.37}_{-0.77}$	$^{+0.19}_{-0.13}$
NLO+NLL	7.09	$^{+0.28}_{-0.51}$	$^{+0.19}_{-0.13}$
NNLO+NNLL	7.35	$^{+0.11}_{-0.21}$	$^{+0.17}_{-0.12}$

B. Experimental final states

In the SM, the top quark decays through the weak interaction into a W^+ boson and a down-type quark, where decays into W^+s and W^+d are expected to be suppressed

Operated by Fermi Research Alliance, LLC under Contract No. De-AC02-07CH11359 with the United States Department of Energy.

relative to W^+b by the square of the Cabibbo-Kobayashi-Maskawa [27] matrix elements V_{ts} and V_{td}. Hence, the decay $t \to W^+b$, and its charge conjugate, is expected to occur with a branching fraction above $\approx 99.8\%$. The W^+ boson subsequently decays either leptonically into $e^+\nu_e$, $\mu^+\nu_\mu$, or $\tau^+\nu_\tau$; or into $u\bar{d}$ or $c\bar{s}$ quarks [28]. All the quarks in the final state evolve into jets of hadrons. In studies of $t\bar{t} \to W^+bW^-\bar{b}$, different final states are defined by the decays of the two W bosons. The main channels are the following:

(i) Dilepton: Events where both W bosons decay into $e\nu_e$, $\mu\nu_\mu$, or $\tau\nu_\tau$ with the τ decaying leptonically, comprise the dilepton channel. While the branching fraction for this channel is only about 4%, its analysis benefits from having a low background.

(ii) Lepton+jets: This channel (ℓ+jets) consists of events where one W boson decays into quarks and the other into $e\nu_e$, $\mu\nu_\mu$, or $\tau\nu_\tau$ with the τ decaying leptonically. The branching fraction of this channel is approximately 35%. The main background contribution is from the production of W bosons in association with jets.

(iii) All-jets: Events where both W bosons decay into quarks form the channel with the largest branching fraction of about 46%. Experimentally, this channel suffers from a large background contribution from multijet production.

The remaining two channels are from final states where at least one of the W bosons decays into $\tau\nu_\tau$ with the τ decaying into hadrons and ν_τ. These channels have larger uncertainties, because of the difficulty of reconstructing the hadronic τ decays. Hence, they are not used in this combination.

C. Selection and modeling

The measurement of the $t\bar{t}$ production cross section in each individual final state requires specific event-selection criteria to enrich the $t\bar{t}$ content of each sample, a detailed understanding of background contributions, as well as good modeling of the SM expectation for the signal and for all background processes. This section briefly discusses these essential ingredients. The CDF II and D0 detectors are described in Refs. [29] and [30], respectively.

1. Event selection

Candidate $t\bar{t}$ events are collected by triggering on leptons of large transverse momentum (p_T), and on characteristics of ℓ+jets or multijet events that depend on the specific final state. Differences in topology and kinematic properties between $t\bar{t}$ events and background processes in each final state are exploited to enrich the $t\bar{t}$ content of the data samples. The discriminating observables used at CDF and D0 for these selections are based on the properties of jets, electrons, muons, and the imbalance in transverse momentum ($\not\!\!p_T$) in such events. At D0, jets are reconstructed using an iterative midpoint jet cone algorithm [31] with $\mathcal{R} = 0.5$ [32], while CDF uses a similar algorithm [33] with $\mathcal{R} = 0.4$. Electrons are reconstructed using information from the electromagnetic calorimeter, and also require a track from the central tracker that is matched to the energy cluster in the calorimeter. Muons are reconstructed using information from the muon system, and also require a matching track from the central tracker. Isolation criteria are applied to identify electrons and muons from $W \to \ell\nu_\ell$ decays. The reconstructed primary interaction vertex must be within 60 cm of the longitudinal center of the detector, corresponding to about 95% of the luminous region.

A common feature of all $t\bar{t}$ events are the two b-quark jets from $t \to Wb$ decays. The $t\bar{t}$ content of the selected event samples can therefore be enriched by demanding that they contain identified b jets. At CDF, b jets are identified through the presence of a displaced, secondary vertex [34], while at D0, a neural-network (NN) based b-jet identification algorithm is used for this purpose [35]. The NN-based algorithm combines the information about the impact parameters of charged particle tracks and the properties of reconstructed secondary vertices into a single discriminant.

The $\not\!\!p_T$ is reconstructed using the energy deposited in calorimeter cells, incorporating corrections for the p_T of leptons and jets. More details on identification criteria for these quantities at CDF and D0 can be found in Ref. [36].

General topologies of each of the three channels are described below, with specific selections described in the respective references to the individual measurements cited in Sec. II. The selections are designed so that the channels are mutually exclusive.

(i) Dilepton candidates are selected by requiring at least two central jets with high p_T; two high-p_T, isolated leptons of opposite charge; and large $\not\!\!p_T$ to account for the undetected neutrinos from the $W \to \ell\nu_\ell$ decays. Other selections based on the global properties of the event are applied to reduce backgrounds in each of the e^+e^-, $e^\pm\mu^\mp$, and $\mu^+\mu^-$ final states.

(ii) ℓ+jets candidates must have at least three high-p_T jets; one high-p_T, isolated electron or muon within a fiducial region; and significant $\not\!\!p_T$ to account for the undetected neutrino from the $W \to \ell\nu_\ell$ decay. In addition, requirements are applied on the azimuthal angle between the lepton direction and $\not\!\!p_T$, to reduce contributions from multijet background.

(iii) All-jets candidates must have at least six central jets with large p_T. Events containing an isolated electron or muon are vetoed, and the event $\not\!\!p_T$ has

Operated by Fermi Research Alliance, LLC under Contract No. De-AC02-07CH11359 with the United States Department of Energy.

to be compatible with its resolution as there are no neutrinos from the W boson decays in this final state.

2. Modeling of signal

A top-quark mass of $m_t = 172.5$ GeV, which is close to the measured top-quark mass [3], is used in the simulation of $t\bar{t}$ production. Several other values are also simulated in order to describe the dependence of the measurement of $\sigma_{t\bar{t}}$ on the assumed value of m_t in the simulation. This dependence is described in Sec. IV.

All of the experimental measurements use LO simulations to predict the fraction of $t\bar{t}$ production passing the selection requirements and to model the kinematic properties of $t\bar{t}$ production. These quantities are less sensitive to higher-order QCD corrections than the absolute rate. Contributions to the systematic uncertainty from $t\bar{t}$ modeling are estimated to be approximately 1% due to the effect of higher-order QCD corrections. At D0, $t\bar{t}$ production and decay are simulated using the ALPGEN program [37]. Parton showering and hadronization are simulated using the PYTHIA [38] program. Double-counting of partonic event configurations is avoided by using a jet-parton matching scheme [39]. The generated events are subsequently processed through a GEANT-based [40] simulation of the D0 detector. The presence of additional $p\bar{p}$ interactions is modeled by overlaying data from random $p\bar{p}$ crossings on the events. At CDF, $t\bar{t}$ events are simulated using standalone PYTHIA, and subsequently processed through a GEANT-based simulation of the CDF II detector [41, 42], with additional $p\bar{p}$ collisions modeled using simulation. Finally, the events are reconstructed with the same algorithms as used for data. Both collaborations implement additional correction factors to take into account any differences between data and simulation. In particular, corrections are made to the jet-energy scale, jet-energy resolution, electron and muon energy scales, trigger efficiencies, and b-jet identification performance [15, 43–46]. At D0, the CTEQ6L1 PDF set is used for event generation [47], while CDF uses the CTEQ6.6 [17] or CTEQ5L PDF parametrizations [48].

3. Modeling of backgrounds

Different sources of backgrounds contribute to different final states. In the dilepton channel, the dominant source of background is from Drell-Yan production of Z bosons or virtual photons through $q\bar{q} \to Z$ or γ^* and associated jets, with the Z/γ^* decaying into a pair of leptons. In addition, electroweak diboson production (WW, WZ, and ZZ) and instrumental background arising from multijet and W+jets production, where a jet is misidentified as a lepton, contribute to the dilepton final state. At CDF, $W\gamma$ production is considered separately, while at D0 this contribution is included in the instrumental background when the γ is misidentified as a lepton or as a jet. For ℓ+jets final states, the major background contribution is from W+jets production, where the W boson decays into $\ell\nu_\ell$. Backgrounds from single top-quark production, diboson production, Z/γ^*+jets, and multijet production are also considered. The dominant background contribution to all-jets events is from multijet production processes.

Contributions from Z/γ^*+jets and W+jets backgrounds are modeled using ALPGEN, followed by PYTHIA for parton showering and hadronization. Contributions from heavy flavor (HF) quarks, namely from $W + b\bar{b}$, $W + c\bar{c}$, $W + c$, $Z/\gamma^* + b\bar{b}$, and $Z/\gamma^* + c\bar{c}$ are simulated separately.

The diboson contributions to dilepton and ℓ+jets final states are simulated using standalone PYTHIA, normalized to the NLO cross section calculated using MCFM [49]. Single top-quark contributions are simulated using the COMPHEP generator [50] at D0, and MADEVENT [51] at CDF, and normalized to the approximate NNNLO [52] and NLO [53] predictions, respectively. The separate background contribution from $W\gamma$ production at CDF is simulated using the BAUR program [54].

The instrumental and multijet backgrounds are estimated using data-driven methods in different ways for each final state at CDF and D0.

II. CDF AND D0 COMBINATIONS

We present the first combination of four CDF measurements, which gives the most precise CDF result to date, and then review the result of a published combination of two D0 measurements.

A. CDF measurements and their combination

CDF includes four measurements in the combination: one from the dilepton channel [43], two from the lepton+jets channel [44], and one from the all-jets channel [45]. Table II summarizes these CDF measurements of $\sigma_{t\bar{t}}$ and their uncertainties. A detailed description of the sources of systematic uncertainty and their correlations is given in Section III.

The dilepton (DIL) measurement, $\sigma_{t\bar{t}} = 7.09 \pm 0.83$ pb, relies on counting events with at least one identified b jet, and uses the full Run II data set corresponding to an integrated luminosity of 8.8 fb^{-1} [43]. Backgrounds from diboson and Z/γ^* events are predicted from simulation, with additional correction factors extracted from control samples in data. The largest systematic uncertainties for this measurement are from the luminosity and the modeling of the detector's b-jet identification.

The two CDF measurements in the ℓ+jets channel are based on 4.6 fb^{-1} of data and apply complementary methods to discriminate signal from background [44].

Operated by Fermi Research Alliance, LLC under Contract No. De-AC02-07CH11359 with the United States Department of Energy.

TABLE II: CDF measurements of $\sigma_{t\bar{t}}$ and their combination (in pb), with individual contributions to their uncertainties (in pb).

	DIL	LJ-ANN	LJ-SVX	HAD	CDF combined
Central value of $\sigma_{\bar{t}t}$	7.09	7.82	7.32	7.21	7.63
Sources of systematic uncertainty					
Modeling of the detector	0.39	0.11	0.34	0.41	0.17
Modeling of signal	0.23	0.23	0.23	0.44	0.21
Modeling of jets	0.23	0.23	0.29	0.71	0.21
Method of extracting $\sigma_{t\bar{t}}$	0.00	0.01	0.01	0.08	0.01
Background modeled from theory	0.01	0.13	0.29	–	0.10
Background based on data	0.15	0.07	0.11	0.59	0.08
Normalization of Z/γ^* prediction	–	0.16	0.15	–	0.13
Luminosity: inelastic $p\bar{p}$ cross section	0.28	–	–	0.29	0.05
Luminosity: detector	0.30	0.02	0.02	0.30	0.06
Total systematic uncertainty	0.67	0.41	0.61	1.18	0.39
Statistical uncertainty	0.49	0.38	0.36	0.50	0.31
Total uncertainty	0.83	0.56	0.71	1.28	0.50

The first measurement, $\sigma_{t\bar{t}} = 7.82 \pm 0.56$ pb, uses an artificial neural network to exploit differences between the kinematic properties of signal and W+jets background, without employing b-jet identification. This analysis is referred to as LJ-ANN. Due to the large mass of the top quark, its decay products have larger p_T and are more isotropic than the main backgrounds from W+jets and multijet production. Seven kinematic properties are selected for analysis in an artificial NN in order to minimize the statistical uncertainty and the systematic uncertainty from the calibration of the jet energy. Since W+jets production is the dominant background in the ℓ+jets channel before the application of b-jet identification requirements, the NN is trained using only $t\bar{t}$ and W+jets simulated samples. The number of $t\bar{t}$ events is then extracted from a maximum likelihood fit to the distribution of NN output in data with three or more jets. The largest systematic uncertainties are from the calibration of jet energy and the modeling of the $t\bar{t}$ signal.

The second ℓ+jets measurement, $\sigma_{t\bar{t}} = 7.32 \pm 0.71$ pb, suppresses the dominant W+jets background by reconstruction of displaced secondary vertices to identify b jets. This analysis is referred to as LJ-SVX. The $\sigma_{t\bar{t}}$ is extracted from a maximum likelihood fit to the observed number of events in data with at least one identified b jet, given the predicted background. The W+HF contribution is determined by applying the b-jet identification efficiency and a corrected HF fraction to an estimate of W+jets before b-jet identification. The HF fraction predicted by the simulation is an underestimate of the yield in data, and a correction factor is derived from a data control sample. The estimate of W+jets is the number of observed events in data before b-jet identification minus the contribution from other processes ($t\bar{t}$, multijet, single-top, diboson, and Z/γ^*+jets). The contribution from events with jets misidentified as b jets is found by applying a parameterized probability function to the data before the b-jet identification requirement. The largest systematic uncertainties in this method arise from the correction for the W+HF background and the modeling of the b-jet identification efficiency.

Both ℓ+jets measurements reduce the uncertainty from luminosity by using the ratio of the $t\bar{t}$ to the Z/γ^* cross sections measured concurrently. This ratio is multiplied by the more precise theoretical prediction for the Z/γ^* cross section [55], thereby replacing the 6% uncertainty on luminosity with a 2% uncertainty from the smaller theoretical and experimental uncertainties on the Z/γ^* cross section.

The ℓ+jets measurements use subsets of events that pass a common selection. Their 32% statistical correlation is evaluated through 1000 simulated experiments. The $\sigma_{t\bar{t}}$ is extracted for each such simulated experiment; for LJ-ANN, through a maximum likelihood fit to the NN distribution, and for LJ-SVX, through the observed number of events with at least one identified b jet in each simulated experiment.

In the all-jets (HAD) measurement, $\sigma_{t\bar{t}} = 7.21 \pm 1.28$ pb, a signal sample is selected by requiring six to eight jets in an event [45]. Additional criteria require the presence of identified b jets and restrictions on the value of a NN discriminant. The latter involves 13 observables as input, and is trained to suppress the large backgrounds from multijet events. To improve the statistical significance of the measurement, the requirement on the value of the discriminant is optimized separately for events with only one b jet and for events with more than one b jet. The $\sigma_{t\bar{t}}$ value is extracted from a simultaneous fit to the reconstructed top-quark mass in both samples. The measurement uses only data corresponding to an integrated luminosity of 2.9 fb^{-1}, but the largest single uncertainty arises from the limited knowledge of the calibration of jet energy.

To combine the CDF measurements, a best linear un-

Operated by Fermi Research Alliance, LLC under Contract No. De-AC02-07CH11359 with the United States Department of Energy.

biased estimate (BLUE) [56–58] is calculated for $\sigma_{t\bar{t}}$ with the goal of minimizing the total uncertainty. A covariance matrix is constructed from the statistical and systematic uncertainties of each result, and from their statistical and systematic correlations. The matrix is inverted to obtain a weight for each result. These weights are applied to the results to obtain the best estimate.

Three iterations of the BLUE combination procedure are performed to eliminate a small bias. For a measurement with N observed events, inspection of the simple expression $\sigma_{t\bar{t}} = (N - B)/(\epsilon\mathcal{L})$ shows that the uncertainty on the background estimate B gives a systematic uncertainty on $\sigma_{t\bar{t}}$ that is independent of the measured value of $\sigma_{t\bar{t}}$. However, the uncertainties on the $t\bar{t}$ selection efficiency ϵ and the luminosity $\mathcal{L}$ produce systematic uncertainties on $\sigma_{t\bar{t}}$ that are directly proportional to the measured value of $\sigma_{t\bar{t}}$. This means that measurements that observe a low value for $\sigma_{t\bar{t}}$ have a smaller systematic uncertainty and a larger weight in the BLUE combination than measurements that observe a high value for $\sigma_{t\bar{t}}$. Hence, the BLUE combination underestimates $\sigma_{t\bar{t}}$ and its uncertainty. This bias is removed by calculating the size of the systematic uncertainties on $\sigma_{t\bar{t}}$ from the $t\bar{t}$ selection efficiency and luminosity by using the BLUE combination value from the previous iteration, instead of each measurement's value of $\sigma_{t\bar{t}}$. The first iteration uses an arbitrary initial value of 6 pb. Simulated experiments show that this procedure removes the bias.

The combined CDF measurement is

$$\sigma_{t\bar{t}}(\text{CDF}) = 7.63 \pm 0.31\,(\text{stat}) \pm 0.36\,(\text{syst}) \pm 0.15\,(\text{lumi})\ \text{pb},$$

for $m_t = 172.5$ GeV. The total uncertainty is 0.50 pb. Table II shows the individual contributions to the uncertainties. The luminosity uncertainty quoted above is the sum in quadrature of two sources of uncertainty, from the inelastic $p\bar{p}$ cross section and from detector-specific effects. The combination has a χ^2 of 0.86 for three degrees of freedom, corresponding to a probability of 84% to have a less consistent set of measurements.

The largest weight in the BLUE combination of CDF measurements is 70% for the ℓ+jets channel LJ-ANN result. The dilepton result has a weight of 22%, and the measurement using b-jet identification in the ℓ+jets channel has a weight of 15%. The measurement in the all-jets channel has a weight of -7%. Such negative weights can occur when the correlation between the two measurements is larger than the ratio of their total uncertainties [56]. The correlation matrix, including statistical and systematic effects, is given in Table III. The largest correlation is 51% between the DIL and HAD measurements, due to the correlation between systematic uncertainties on detector modeling (primarily b-jet identification), signal modeling, jet energy scale, and luminosity. Next largest is the 50% correlation between the LJ-ANN and LJ-SVX measurements, which arises from a subset of common events and correlation between systematic uncertainties from signal modeling, jet energy scale, and normalization of the Z/γ^* cross section. The central value and the total uncertainty change by less than 0.01 pb when the statistical correlation of 32% between the LJ-ANN and LJ-SVX measurements is varied by 10% absolute to 22% or 42%.

TABLE III: Correlation matrix for CDF $\sigma_{t\bar{t}}$ measurements, including statistical and systematic correlations among the methods.

Correlation	LJ-ANN	LJ-SVX	DIL	HAD
LJ-ANN	1	0.50	0.25	0.34
LJ-SVX		1	0.44	0.47
DIL			1	0.51
HAD				1

B. D0 measurements and their combination

D0 includes two measurements in the combination: one from the dilepton channel and one from the ℓ+jets channel. In the dilepton channel, using data corresponding to an integrated luminosity of 5.4 fb^{-1}, D0 measures $\sigma_{t\bar{t}} = 7.36^{+0.90}_{-0.79}$ pb through a likelihood fit to a discriminant based on a NN b-jet identification algorithm [15]. The $\sigma_{t\bar{t}}$ is extracted from a fit to the distribution of the smallest of the NN output values from the two jets of highest energy. The total uncertainty is not limited by the finite sample size but by the systematic uncertainty on the integrated luminosity.

In the ℓ+jets channel, using data corresponding to an integrated luminosity of 5.3 fb^{-1}, D0 measures $\sigma_{t\bar{t}} = 7.90^{+0.78}_{-0.69}$ pb by selecting events with at least three jets and splitting them into subsamples according to the total number of jets and the number of identified b jets [46]. In the background-dominated subsamples (three-jet events with no b jet, three-jet events with one b jet, and events with at least four jets and no b jet), a random forest multivariate discriminant [59] is used to separate signal from background. The $\sigma_{t\bar{t}}$ is extracted by fitting simultaneously the direct event count in the subsamples with a large $t\bar{t}$ content (three-jet events with at least two b jets, events with at least four jets and one b jet, and events with at least four jets and at least two b-jets) and the random forest discriminant in the background-dominated samples. The leading systematic uncertainties are treated as nuisance parameters, constrained by Gaussian prior probability density functions, that are allowed to vary in the fit. The dominant systematic uncertainty is from the uncertainty on the luminosity, followed by uncertainties from the modeling of the detector.

The measurements in the dilepton and ℓ+jets channels have been combined and published in the dilepton paper [15] with the same nuisance-parameter technique used in the individual measurements, accounting for correlations among common systematic sources. The result is $\sigma_{t\bar{t}}(\text{D0}) = 7.56^{+0.63}_{-0.56}$ pb. For the combination with CDF, we separate the statistical and systematic contributions into the categories discussed in the next section.

Operated by Fermi Research Alliance, LLC under Contract No. De-AC02-07CH11359 with the United States Department of Energy.

We also use the average of the asymmetric uncertainties of the original D0 measurement. This gives for the combined D0 measurement

$$\sigma_{t\bar{t}}(\mathrm{D0}) = 7.56 \pm 0.20(\mathrm{stat}) \pm 0.32\,(\mathrm{syst}) \pm 0.46\,(\mathrm{lumi})\ \mathrm{pb},$$

for $m_t = 172.5$ GeV. The total uncertainty is 0.59 pb. Table IV provides the individual contributions to the uncertainties. The luminosity uncertainty quoted above is the sum in quadrature of two sources of uncertainty, from the inelastic $p\bar{p}$ cross section and from detector-specific effects.

III. OVERVIEW OF SYSTEMATIC UNCERTAINTIES

Sources of systematic uncertainty have been categorized into nine classes with similar correlation properties to facilitate the combination of the measurements. Below, we discuss each component of the uncertainty on the combined cross section. The values of the CDF and D0 systematic uncertainties are summarized in Tables II and IV.

A. Modeling of the detector

This category includes detector-specific uncertainties on the trigger and lepton-identification efficiency, b-jet identification efficiency, and modeling of multiple $p\bar{p}$ interactions. In addition, for CDF measurements, this category includes the uncertainty on the fraction of the luminous region within the acceptance of the CDF II detector, track-identification efficiencies for the LJ-ANN and LJ-SVX measurements, and the uncertainty on the lepton-energy scales. For D0 measurements, additional uncertainties in this category arise from vertex reconstruction and identification efficiency and lepton-energy resolution. These sources are treated as correlated within the same experiment, but uncorrelated between experiments.

B. Modeling of signal

The uncertainties in this category arise from several sources and are considered fully correlated among all measurements.

(i) $t\bar{t}$ generator: This is the source of the largest contribution ($1-2\%$) to the signal modeling systematic. For both CDF and D0 measurements this uncertainty includes the difference between PYTHIA and HERWIG [60] samples resulting from different models for hadronization, for parton showering and for the underlying event, which describes the remnants of the p and $\bar{p}$ break-up accompanying the hard partonic collision. Uncertainties from higher-order QCD corrections are also included for D0 measurements by comparing results from ALPGEN to MC@NLO [61]. Although there are reported measurements of a larger-than-expected forward-backward asymmetry [62, 63] that could be due to non-SM sources, no additional systematic is assigned as its size would be highly dependent on the particular hypothesis for the source.

(ii) Parton distribution functions: The uncertainties on the PDF reflect the uncertainty on determining the probability of finding a particular parton carrying a particular fraction of the p or $\bar{p}$ momentum. This in turn affects the kinematic distributions of the final-state particles in $t\bar{t}$ production and decay, as well as the event selection efficiency. The default acceptances are calculated using the LO CTEQ5L and CTEQ6L PDF sets for CDF and D0, respectively. The systematic uncertainty includes uncertainties evaluated using the prescribed NLO error vectors from CTEQ6M for CDF, and CTEQ6.1M for D0, following the recommendations of the CTEQ collaboration [64]. For CDF measurements, this uncertainty also includes the difference between the central values from LO and NLO PDF [65].

(iii) Initial and final-state radiation: The amount of gluon radiation from partons in the initial or final state, which affects the $t\bar{t}$ efficiency and kinematic properties, is set by parameters of the PYTHIA generator used to simulate $t\bar{t}$ events. The uncertainties on these parameters are taken from a study of initial state radiation in Drell-Yan events, $q\bar{q} \to Z/\gamma^* \to \mu^+\mu^-$, that share the same initial $q\bar{q}$ state as most of the $t\bar{t}$ signal [65, 66].

(iv) Color reconnection: This uncertainty is evaluated by comparing PYTHIA configurations with different parameters that affect the exchange of momentum and energy via gluons between the color-connected top-quark and antitop-quark systems. Specifically, the difference in $t\bar{t}$ efficiency obtained with PYTHIA using the A-PRO and the ACR-PRO configurations [67] is quoted as the systematic uncertainty [65].

(v) Leptonic decay branching fractions for W bosons: This uncertainty alters the proportion of $t\bar{t}$ decays that cause the dilepton, ℓ+jets, and all-jets final states. It is evaluated by changing the branching fractions in the W-boson decay by their uncertainties [27].

C. Modeling of jets

Uncertainties on the modeling of jets affect the $t\bar{t}$ selection efficiency and the kinematic distributions used to extract $\sigma_{t\bar{t}}$. They arise from the calibration of light-quark

and b-jet energies, and modeling of jet reconstruction and resolution in the simulation. These sources are treated as correlated within each experiment, and uncorrelated between experiments.

(i) Jet-energy scale: This uncertainty arises from uncertainties in calibrating jet energy using test-beam data (CDF), as well as γ+jets and dijet events (CDF and D0). The effect on the measurement is evaluated by replacing the jet energies in the nominal simulated samples with energies changed by their estimated systematic uncertainties.

(ii) b-jet energy scale: This uncertainty accounts for the difference in energy between jets originating from light-flavor quarks or gluons, and from b quarks. For CDF, it includes uncertainties on branching fractions of semileptonic decays of b and c quarks; uncertainties on b-quark fragmentation; and the uncertainty on the calorimeter response to b and c hadrons. For D0, the sources are uncertainties on parameters for b-quark fragmentation, and the difference in calorimeter response to jets from b and light quarks. More details can be found in Ref. [65].

(iii) Jet reconstruction and identification: This uncertainty is specific to D0 results, and covers the uncertainty on correction factors applied to simulation to match the jet identification efficiency in data, and on factors used to adjust the jet resolution in simulation to that observed in data.

D. Method for extracting $\sigma_{t\bar{t}}$

This uncertainty is different for each method, and arises from the limited size of the simulated samples or from the dependence of the calibration on the specific analysis. It is uncorrelated among all measurements.

E. Background modeled from theory

For both experiments, this uncertainty includes the uncertainty on the heavy-flavor fraction in W+jets events, uncertainties on the normalization of the electroweak background (diboson and single top-quark production), and the dependence on the renormalization and factorization scale in W+jets simulation. Details about specific modeling of background and the treatment of systematic uncertainties are in the references for each individual measurement. Since these uncertainties are related to the theoretical description of the background, this source is treated as correlated among all measurements.

F. Background based on data

This source covers uncertainties on multijet background in both experiments; the uncertainty in the modeling of the Z/γ^*+jets background, obtained from data by D0; and uncertainties on misidentification of jets from charm and light-flavor quarks as b jets at CDF. This source is considered uncorrelated among all measurements.

G. Normalization of Z/γ^* predictions

This uncertainty is applicable only to the LJ-ANN and LJ-SVX measurements by CDF, which exploit the ratio of observed $t\bar{t}$ to Z/γ^* production and therefore involve the normalization using the predicted Z/γ^* cross section [55]. It includes the uncertainty on the predicted Z/γ^*+jets cross section, and the contributions to the uncertainty on the measured Z/γ^*+jets cross section from the background estimate, and from the choice of renormalization and factorization scale for the Z/γ^*+jets simulation.

H. Luminosity uncertainty

The luminosity uncertainty has two sources:

(i) Inelastic $p\bar{p}$ cross section: The total inelastic $p\bar{p}$ cross section [68] has an uncertainty of 4.0%. This source is correlated among all measurements but does not affect the CDF LJ-ANN and LJ-SVX measurements, which exploit the ratio of $t\bar{t}$ to Z/γ^* production rates.

(ii) Detector-specific luminosity uncertainty: This contribution is from detector effects and is approximately 4.5% [69]. This source is treated as correlated for measurements within the same experiment, and uncorrelated between experiments. This uncertainty is negligible for CDF LJ-ANN and LJ-SVX measurements, which exploit the ratio of production rates.

IV. RESULTS

The CDF and D0 $\sigma_{t\bar{t}}$ measurements are combined using the BLUE method described in Sec. II, with inputs from the first two columns of Table IV, yielding the Tevatron average of

$$\sigma_{t\bar{t}} = 7.60 \pm 0.20\,(\text{stat}) \pm 0.29\,(\text{syst}) \pm 0.21\,(\text{lumi})\ \text{pb},$$

assuming $m_t = 172.5$ GeV. The total uncertainty is 0.41 pb. The luminosity uncertainty quoted above is the sum in quadrature of two sources of uncertainty, from the inelastic $p\bar{p}$ cross section and from detector-specific

Operated by Fermi Research Alliance, LLC under Contract No. De-AC02-07CH11359 with the United States Department of Energy.

effects. The individual contributions to the systematic uncertainties are given in the last column of Table IV. The CDF measurement has a weight of 60%, while the D0 measurement has a weight of 40%. The correlation between the measurements of the two experiments is 17%.

The measurements and the Tevatron combination are shown in Figure 1, as well as the results of the CDF-only and D0-only combinations. The Tevatron combination has a χ^2 of 0.01 for one degree of freedom, corresponding to a probability of 92% to have a less consistent set of measurements.

The measured $\sigma_{t\bar{t}}$ depends on the value of m_t assumed in the simulation. For larger values of m_t, leptons and jets from top-quark decay are more energetic and central, and thus more likely to meet the selection requirements on p_T. The b jets are also more likely to be identified since b-jet identification efficiency tends to increase with increasing jet p_T. Both effects cause the $t\bar{t}$ selection efficiency to increase asymptotically to its maximum value as the value of m_t assumed in the simulation increases. The consequence, for a given data sample, is that the measured $\sigma_{t\bar{t}}$ decreases as the assumed value of m_t increases. The dependence on m_t is enhanced for methods that exploit the differences in kinematic properties between $t\bar{t}$ and background, as the discrimination improves as m_t increases. The consequence, for a given data sample, is that these methods will identify a smaller $t\bar{t}$ content, and measure smaller $\sigma_{t\bar{t}}$, as the assumed value of m_t increases in the simulation used to describe $t\bar{t}$ kinematic properties.

Therefore, we also measure $\sigma_{t\bar{t}}$ for several m_t values at which each experiment has simulated $t\bar{t}$ production and decay. At D0, the fit procedure is repeated for each m_t value, using systematic uncertainties extrapolated from the central $m_t = 172.5$ GeV. At CDF, the DIL and LJ-SVX counting measurements extract the selection efficiency for each m_t value, and scale $\sigma_{t\bar{t}}$ by the ratio relative to that from $m_t = 172.5$ GeV. The LJ-ANN and HAD measurements also repeat the fit procedure for each m_t value. We repeat the combination process for CDF and D0, and present the results of the Tevatron combination for $\sigma_{t\bar{t}}$ at three m_t values in Table V. Relative to the central value at m_t of 172.5 GeV, the measured $\sigma_{t\bar{t}}$ increases by 5% for an assumed m_t of 170 GeV, and decreases by 3% for an assumed m_t of 175 GeV. This non-linear dependence is due to the slowing of the rate of increase of the $t\bar{t}$ selection efficiency as m_t increases. We parametrize this dependence through the functional form

$$\sigma_{t\bar{t}} = a + b(m_0 - m_t) + c(m_0 - m_t)^2, \qquad (1)$$

with $m_0 = 172.5$ GeV and fitted values of $a = 7.60$ pb, $b = 0.126$ pb/GeV and $c = 0.0136$ pb/GeV^2. The parameters for the fit corresponding to an upward change of one standard deviation in $\sigma_{t\bar{t}}$ are $a = 8.01$ pb, $b = 0.132$ pb/GeV and $c = 0.0144$ pb/GeV^2, and for a downward change of one standard deviation are $a = 7.19$ pb, $b = 0.120$ pb/GeV and $c = 0.0128$ pb/GeV^2.

The dependence of the measured $\sigma_{t\bar{t}}$ on the value for m_t assumed in the simulation is shown by the shaded band in Fig. 2. The measured $\sigma_{t\bar{t}}$ is in good agreement with the NNLO theoretical prediction for assumed values of m_t below 175 GeV.

V. CONCLUSION

We have presented the combination of measurements of $\sigma_{t\bar{t}}$ in the dilepton, ℓ+jets, and all-jets final states, using data collected by the CDF and D0 collaborations at the Tevatron $p\bar{p}$ collider at $\sqrt{s} = 1.96$ TeV. The measurements use data samples with integrated luminosity between 2.9 fb^{-1} and 8.8 fb^{-1}. Assuming the SM expectation for top-quark decay, we observe good agreement on $\sigma_{t\bar{t}}$ among the different experimental final states. The first combination of the CDF and D0 measurements is

$$\sigma_{t\bar{t}} = 7.60 \pm 0.41 \text{ pb},$$

for a top-quark mass of $m_t = 172.5$ GeV. The combined $\sigma_{t\bar{t}}$ of 7.60 pb has a relative uncertainty of 5.4%, which is close to the relative uncertainty of the prediction from theory of about 4%. The result is in good agreement with the latest theoretical expectation for $\sigma_{t\bar{t}}$ in the standard model, calculated at NNLO+NNLL QCD, of $7.35^{+0.28}_{-0.33}$ pb [24], as presented in Fig. 2.

In the future, two improvements to the individual measurements could reduce the total uncertainty on the combined result by about 25% to 0.31 pb. Firstly, the D0 measurements and the CDF ℓ+jets channel measurements could have their statistical uncertainties reduced by a factor of about 1.4 by updating the published analyses from 5 fb^{-1} to the full integrated luminosity of about 10 fb^{-1} of data collected in Run II. Secondly, the D0 measurements and the CDF dilepton channel measurement could also reduce their luminosity uncertainty, as done by the CDF ℓ+jets channel measurements, by using the ratio of the $t\bar{t}$ to the Z/γ^* cross sections measured concurrently and then multiplying by the more precisely known theoretical prediction for the Z/γ^* cross section. This strategy would reduce the current 6% luminosity uncertainty to a 2% systematic uncertainty on the normalization of the Z/γ^* prediction.

Acknowledgments

We thank the Fermilab staff and technical staffs of the participating institutions for their vital contributions. We acknowledge support from the DOE and NSF (USA), ARC (Australia), CNPq, FAPERJ, FAPESP and FUNDUNESP (Brazil), NSERC (Canada), NSC, CAS and CNSF (China), Colciencias (Colombia), MSMT and GACR (Czech Republic), the Academy of Finland, CEA and CNRS/IN2P3 (France), BMBF and DFG (Germany), DAE and DST (India), SFI (Ireland), INFN

TABLE IV: CDF and D0 measurements of $\sigma_{t\bar{t}}$ and their combination (in pb), with individual contributions to their uncertainties (in pb). Correlation indicates whether a given uncertainty is treated as fully correlated between the CDF and D0 measurements.

	CDF	D0		Tevatron
Central value of $\sigma_{t\bar{t}}$	7.63	7.56		7.60
Sources of systematic uncertainty			Correlation	
Modeling of the detector	0.17	0.22	NO	0.13
Modeling of signal	0.21	0.13	YES	0.18
Modeling of jets	0.21	0.11	NO	0.13
Method of extracting $\sigma_{t\bar{t}}$	0.01	0.07	NO	0.03
Background modeled from theory	0.10	0.08	YES	0.10
Background based on data	0.08	0.06	NO	0.05
Normalization of Z/γ^* prediction	0.13	–	NO	0.08
Luminosity: inelastic $p\bar{p}$ cross section	0.05	0.30	YES	0.15
Luminosity: detector	0.06	0.35	NO	0.14
Total systematic uncertainty	0.39	0.56		0.36
Statistical uncertainty	0.31	0.20		0.20
Total uncertainty	0.50	0.59		0.41

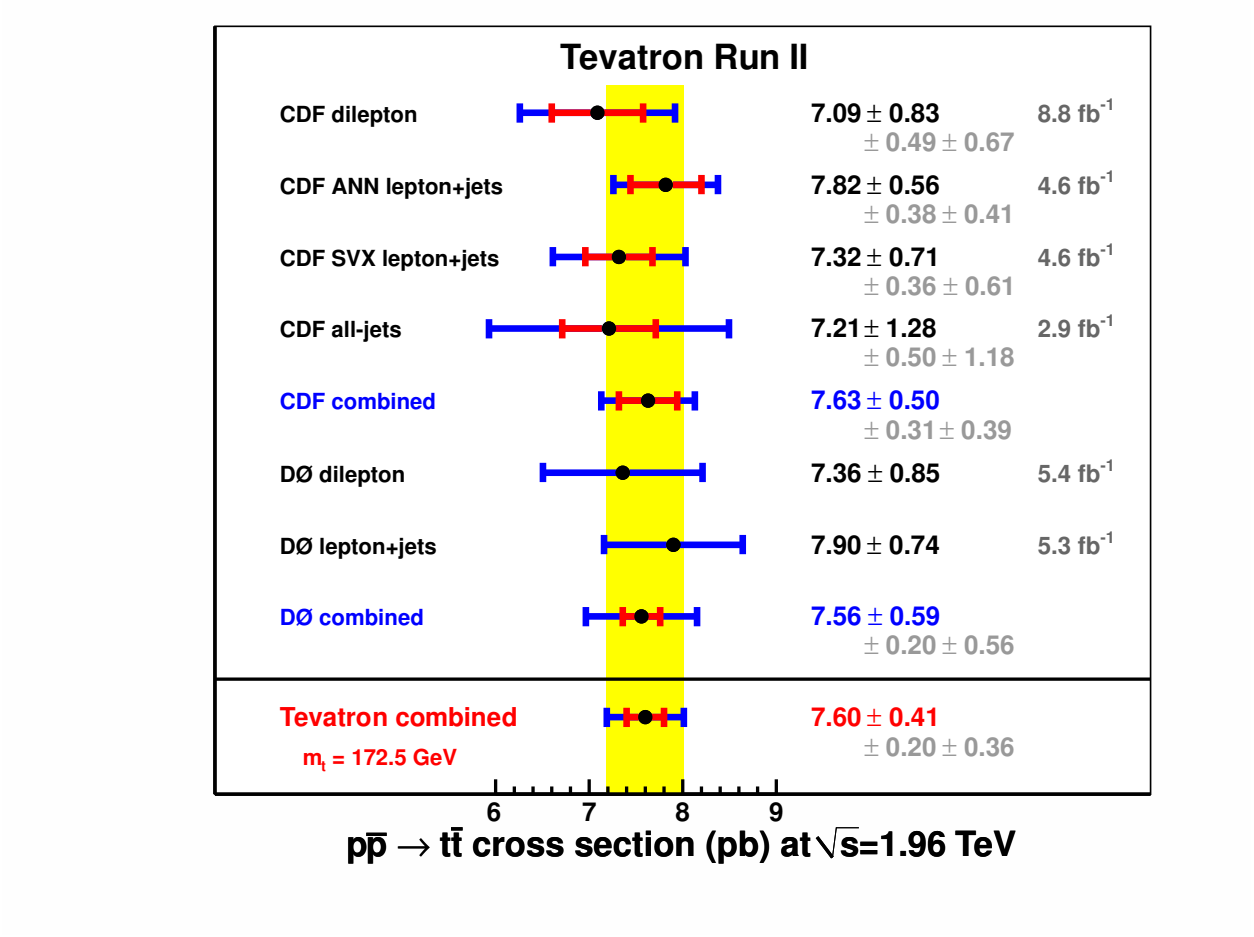

FIG. 1: (color online). The six input $\sigma_{t\bar{t}}$ measurements from the CDF and D0 experiments, along with the CDF-only and D0-only combination results, and their combination for the Tevatron result. The total uncertainty, as well as the statistical and systematic uncertainties are shown. The D0 dilepton and ℓ+jets measurements using constrained nuisance parameters are presented in their published form indicating only their total uncertainties. The inner (red) bars reflect statistical uncertainties while the outer (blue) bars show the total uncertainties on each measurement.

Operated by Fermi Research Alliance, LLC under Contract No. De-AC02-07CH11359 with the United States Department of Energy.

TABLE V: CDF and D0 measurements of $\sigma_{t\bar{t}}$ and their combination, with total uncertainties, for three values of m_t.

Top-quark mass (GeV)	170	172.5	175
CDF $\sigma_{t\bar{t}}$ (pb)	8.17 ± 0.53	7.63 ± 0.50	7.35 ± 0.48
D0 $\sigma_{t\bar{t}}$ (pb)	7.75 ± 0.61	7.56 ± 0.59	7.40 ± 0.57
Tevatron $\sigma_{t\bar{t}}$ (pb)	8.00 ± 0.43	7.60 ± 0.41	7.37 ± 0.40

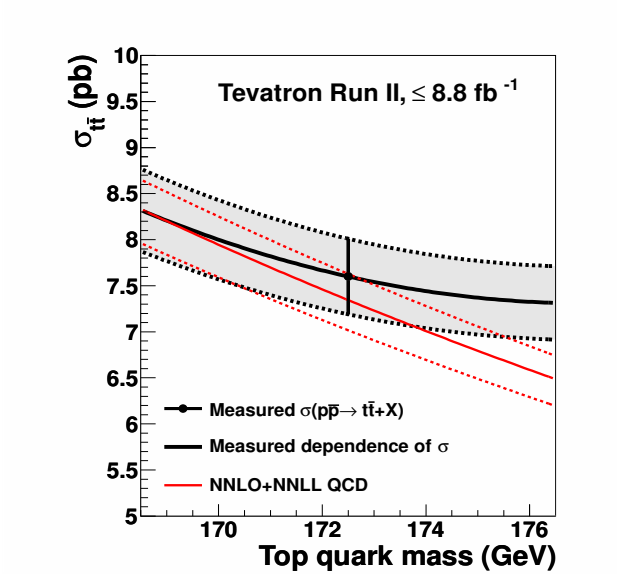

FIG. 2: (color online). The combined $\sigma_{t\bar{t}}$ at the Tevatron as a function of m_t (black line), as expressed by Eq.(1), compared to the prediction (narrower red line) at NNLO+NNLL in perturbative QCD [24]. The dashed lines show the total uncertainty on the result (black dashed lines enclosing shaded region) and the prediction (narrower red dashed lines).

(Italy), MEXT (Japan), the Korean World Class University Program and NRF (Korea), CONACyT (Mexico), FOM (Netherlands), MON, NRC KI and RFBR (Russia), the Slovak R&D Agency, the Ministerio de Ciencia e Innovación, and Programa Consolider-Ingenio 2010 (Spain), The Swedish Research Council (Sweden), SNSF (Switzerland), STFC and the Royal Society (United Kingdom), the A.P. Sloan Foundation (USA), and the EU community Marie Curie Fellowship contract 302103.

[1] F. Abe *et al.* (CDF Collaboration), Phys. Rev. Lett. **74**, 2626 (1995).
[2] S. Abachi *et al.* (D0 Collaboration), Phys. Rev. Lett. **74**, 2632 (1995).
[3] T. Aaltonen *et al.* (CDF and D0 Collaborations), arXiv:1305.3929; consistent with J. Beringer *et al.* (Particle Data Group), Phys. Rev. D **86**, 010001 (2012).
[4] T. Aaltonen *et al.* (CDF Collaboration), Phys. Rev. Lett. **102**, 042001 (2009); T. Aaltonen *et al.* (CDF Collaboration), Phys. Rev. Lett. **105**, 232003 (2010); V.M. Abazov *et al.* (D0 Collaboration), Phys. Rev. Lett. **106**, 022001 (2011); V.M. Abazov *et al.* (D0 Collaboration), Phys. Rev. D **85**, 091104 (2012).
[5] M. Jeżabek and J.H. Kühn, Phys. Rev. D **48**, 191 (1993).
[6] G. Aad *et al.* (ATLAS Collaboration), Phys. Lett. B **716**, 1 (2012).
[7] S. Chatrchyan *et al.* (CMS Collaboration), Phys. Lett. B **716**, 30 (2012).
[8] G. Degrassi *et al.* , J. High Energy Phys. 08 (2012) 098.
[9] T. Aaltonen *et al.* (CDF Collaboration), Phys. Rev. Lett. **110**, 121802 (2013). T. Aaltonen *et al.* (CDF Collaboration), Phys. Rev. D **84**, 072004 (2011); T. Aaltonen *et al.* (CDF Collaboration), Phys. Rev. D **84**, 072003 (2011); T. Aaltonen *et al.* (CDF Collaboration), Phys. Rev. D **77**, 051102 (2008); T. Aaltonen *et al.* (CDF Collaboration), Phys. Lett. B **691**, 183 (2010).
[10] V. M. Abazov *et al.* (D0 Collaboration), Phys. Rev. D **85**, 051101 (2012); V. M. Abazov *et al.* (D0 Collaboration), Phys. Lett. B **668**, 98 (2008).
[11] T. Aaltonen *et al.* (CDF Collaboration), Phys. Rev. Lett. **103**, 101803 (2009); A. Abulencia *et al.* (CDF Collaboration), Phys. Rev. Lett. **96**, 042003 (2006).
[12] V. M. Abazov *et al.* (D0 Collaboration), Phys. Lett. B **682**, 278 (2009); V. M. Abazov *et al.* (D0 Collaboration), Phys. Rev. D **80**, 071102 (2009); V. M. Abazov *et al.* (D0 Collaboration), Phys. Rev. D **80**, 051107 (2009).
[13] G. Aad *et al.* (ATLAS Collaboration), J. High Energy Phys. 05 (2012) 059.
[14] S. Chatrchyan *et al.* (CMS Collaboration), J. High Energy Phys. 11 (2012) 067.
[15] V. M. Abazov *et al.* (D0 Collaboration), Phys. Lett. B **704**, 403 (2011).
[16] P. Nason, S. Dawson and R. K. Ellis, Nucl. Phys. **B303**, 607 (1988); W. Beenakker, H. Kuijf, W. L. van Neerven and J. Smith, Phys. Rev. D **40**, 54 (1989).
[17] P. M. Nadolsky, H. L. Lai, Q.-H. Cao, J. Huston,

Operated by Fermi Research Alliance, LLC under Contract No. De-AC02-07CH11359 with the United States Department of Energy.

J. Pumplin, D. Stump, W.-K. Tung and C.-P. Yuan, Phys. Rev. D **78**, 013004 (2008).
[18] R. Bonciani, S. Catani, M. L. Mangano and P. Nason, Nucl. Phys. **B529**, 424 (1998) [Erratum-ibid. **B803**, 234 (2008)].
[19] M. Cacciari, S. Frixione, M. L. Mangano, P. Nason and G. Ridolfi, J. High Energy Phys. 04 (2004) 068.
[20] V. Ahrens, A. Ferroglia, M. Neubert, B. D. Pecjak, and L. L. Yang, J. High Energy Phys. 09 (2010) 097; V. Ahrens, A. Ferroglia, M. Neubert, B. D. Pecjak, and L. L. Yang, Nucl. Phys. Proc. Suppl. **205-206**, 48 (2010); V. Ahrens, A. Ferroglia, M. Neubert, B. D. Pecjak, and L. L. Yang, Phys. Lett. B **703**, 135 (2011).
[21] S. Moch and P. Uwer, Phys. Rev. D **78**, 034003 (2008); U. Langenfeld, S. Moch, and P. Uwer, Phys. Rev. D **80**, 054009 (2009); S. Moch, P. Uwer and A. Vogt, Phys. Lett. B **714**, 48 (2012).
[22] N. Kidonakis and R. Vogt, Phys. Rev. D **68**, 114014 (2003); N. Kidonakis, Phys. Rev. D **82**, 114030 (2010); N. Kidonakis, arXiv:1109.3231.
[23] M. Cacciari, M. Czakon, M. L. Mangano, A. Mitov and P. Nason, Phys. Lett. B **710**, 612 (2012).
[24] M. Czakon, P. Fiedler and A. Mitov, arXiv:1303.6254.
[25] M. Czakon and A. Mitov, arXiv:1112.5675.
[26] A. D. Martin, W. J. Stirling, R. S. Thorne and G. Watt, Eur. Phys. J. C **63**, 189 (2009).
[27] J. Beringer *et al.* (Particle Data Group), Phys. Rev. D **86**, 010001 (2012).
[28] Here W^+ also refers to the charge conjugate state with the fermion charges conjugated as well. In the following the charges of the W boson and the leptons ℓ are dropped.
[29] D.E. Acosta *et al.* (CDF Collaboration), Phys. Rev. D **71**, 052003 (2005).
[30] V.M. Abazov *et al.* (D0 Collaboration), Nucl. Instrum. Methods A **565**, 463 (2006).
[31] G.C. Blazey *et al.*, Proceedings of the Workshop on QCD and Weak Boson Physics in Run II, edited by U. Baur, R.K. Ellis, and D. Zeppenfeld, pp. 47–77, (Fermilab, Batavia, 2000), FERMILAB-PUB-00-297.
[32] $\mathcal{R}$ is defined as $\mathcal{R} = \sqrt{(\Delta\eta)^2 + (\Delta\phi)^2}$. The pseudorapidity η is a function of the polar angle θ relative to the proton beam: $\eta(\theta) = -\ln[\tan(\theta/2)]$. We distinguish detector η (η_{det}) and collision η, where the former is defined with respect to the center of the detector and the latter relative to the $p\bar{p}$ interaction vertex. The angle ϕ is the azimuthal angle around the beamline.
[33] A. Bhatti *et al.*, Nucl. Instrum. Methods A **566**, 375 (2006).
[34] D. Acosta *et al.* (CDF Collaboration), Phys. Rev. D **71**, 052003 (2005).
[35] V. M. Abazov *et al.* (D0 Collaboration), Nucl. Instrum. Methods A **620**, 490 (2010).
[36] F. Deliot and D. Glenzinski, Rev. Mod. Phys. **84**, 211 (2012).
[37] M. L. Mangano, M. Moretti, F. Piccinini, R. Pittau, and A. D. Polosa, J. High Energy Phys. 07 (2003) 001.
[38] T. Sjöstrand, L. Lönnblad, and S. Mrenna, hep-ph/0308153 (2003); we used version 6.2 (CDF) and 6.3 (D0).
[39] M. L. Mangano, M. Moretti, F. Piccinini, and M. Treccani, J. High Energy Phys. 01 (2007) 013.
[40] R. Brun and F. Carminati, CERN Program Library Long Writeup W5013, 1993 (unpublished).
[41] E. Gerchtein and M. Paulini, arXiv:physics/0306031.
[42] S. Agostinelli *et al.*, Nucl. Instrum. Methods A **506**, 250 (2003).
[43] T. Aaltonen *et al.* (CDF Collaboration), arXiv:1304.7961, submitted to Phys. Rev. Lett.
[44] T. Aaltonen *et al.* (CDF Collaboration), Phys. Rev. Lett. **105**, 012001 (2010).
[45] T. Aaltonen *et al.* (CDF Collaboration), Phys. Rev. D **81**, 052011 (2010).
[46] V. M. Abazov *et al.* (D0 Collaboration), Phys. Rev. D **84**, 012008 (2011).
[47] J. Pumplin, D. R. Stump, J. Huston, H. L. Lai, P. M. Nadolsky and W. -K. Tung, J. High Energy Phys. 07 (2002) 012.
[48] H. L. Lai *et al.* (CTEQ Collaboration), Eur. Phys. J. C **12**, 375 (2000).
[49] J. M. Campbell and R. K. Ellis, Nucl. Phys. Proc. Suppl. **205-206**, 10 (2010).
[50] E. Boos *et al.* (CompHEP Collaboration), Nucl. Instrum. Methods A **534**, 250 (2004).
[51] J. Alwall, P. Demin, S. de Visscher, R. Frederix, M. Herquet, F. Maltoni, T. Plehn, D. L. Rainwater, and T. Stelzer, J. High Energy Phys. 09 (2007) 028.
[52] N. Kidonakis, Phys. Rev. D **74**, 114012 (2006).
[53] B. W. Harris, E. Laenen, L. Phaf, Z. Sullivan, and S. Weinzierl, Phys. Rev. D **66**, 054024 (2002).
[54] U. Baur and E. L. Berger, Phys. Rev. D **41**, 1476 (1990).
[55] A. Abulencia *et al.* (CDF Collaboration), J. Phys. G **34**, 2457 (2007).
[56] L. Lyons, D. Gibaut and P. Clifford, Nucl. Instrum. Methods A **270**, 110 (1988).
[57] L. Lyons, A. Martin and D. Saxon, Phys. Rev. D **41**, 3 (1990).
[58] A. Valassi, Nucl. Instrum. Methods A **500**, 391 (2003).
[59] A. Hoecker *et al.*, arXiv:physics/0703039.
[60] G. Corcella, I. G. Knowles, G. Marchesini, S. Moretti, K. Odagiri, P. Richardson, M. H. Seymour and B. R. Webber, J. High Energy Phys. 01 (2001) 010.
[61] S. Frixione and B.R. Webber, J. High Energy Phys. 06 (2002) 029.
[62] T. Aaltonen *et al.* (CDF Collaboration), Phys. Rev. D **87**, 092002 (2013).
[63] V. M. Abazov *et al.* (D0 Collaboration), Phys. Rev. D **84**, 112005 (2011).
[64] D. Stump, J. Huston, J. Pumplin, W. -K. Tung, H. L. Lai, S. Kuhlmann and J. F. Owens, J. High Energy Phys. 10 (2003) 046.
[65] T. Aaltonen *et al.* (CDF and D0 Collaborations), Phys. Rev. D **86**, 092003 (2012).
[66] A. Abulencia *et al.* (CDF Collaboration), Phys. Rev. D **73**, 032003 (2006).
[67] P. Z. Skands and D. Wicke, Eur. Phys. J. C **52**, 133 (2007); P. Z. Skands, arXiv:0905.3418.
[68] S. Klimenko, J. Konigsberg and T. M. Liss, FERMILAB-FN-0741.
[69] D. Acosta *et al.*, Nucl. Instrum. Methods A **494**, 57 (2002); T. Andeen *et al.*, Report No. FERMILAB-TM-2365, 2007.

Operated by Fermi Research Alliance, LLC under Contract No. De-AC02-07CH11359 with the United States Department of Energy.